TECHNICAL NOTE

Theoretical Analysis and Digital Photoelastic Measurement of Circular Disks Subjected to Partially Distributed Compressions

by K.-M. Hung and C.-C. Ma

ABSTRACT—The disk in diametral compression has been quoted most frequently on developing conventional/digital photoelasticity to illustrate new theories and experimental techniques for several decades. Theoretically, the compression as a concentrated force is more conducive to analysis, but it is impossible to achieve such loading condition experimentally. The distributed compression on a finite area at rim is relatively closer to actual testing and it is complicated to seek an analytical solution. In this paper, we extend the work of Hondros to derive the full-field stress distribution of disk subjected to diametral distributed compression in an explicit functional form. The principal stress difference and principal stress orientation related to isochromatic and isoclinic fringes, respectively, are also expressed in a simple closed form. The maximum shear stress for the whole disk and the validity of using isochromatic fringes to interpret the maximum shear stress are discussed in detail. The isoclinic fringes are compared with theory, and the fringe multiplication isochromatic is compared with simulated image. All of the comparisons are in good agreement with respect to full field.

KEY WORDS—Disk, distributed compression, digital photoelasticity, isochromatics, isoclinics, principal stress

Introduction

The problem of a circular disk subjected to concentrated forces applied at its boundary is frequently used in classical elasticity either to illustrate theories or to estimate experimental data. The stress analysis of the circular disk has been discussed by many authors.[1–4] However, the actual loads in an experiment are not concentrated but distributed over finite portions of the disk. Sanford[5] proposed a method to conversely calculate the isochromatic fringe order from Frochet's full-field solution by employing a least-squares method. Berghaus[6] presented a method combining finite-element results with photoelastic data to estimate the full-field distribution of stress. Haake *et al.*[7] presented a photoelastic device containing a quarter-wave plate and a polarizer to generate six different angular orientations and came up with six images using a CCD.

The experiment of a disk in diametral compression is easy to conduct. In addition, the analytical solution of the full-field stress can be used as a theoretical reference to check the experimental results. However, the problem of the disk in distributed diametral compression is more difficult to analyze than that with concentrated forces. Hondros[8] obtained the full-field stresses in a series solution by using the series expansion technique and applied these solutions to evaluate the Young's modulus and Poisson's ratio of concrete by measuring strain. Instead of using a series solution for full-field stresses, in this paper we continue and extend the work of Hondros to successfully obtain an analytical solution in an explicit form which can provide a full-field sampling capability as well as in-depth theoretical comparisons. Concise mathematical forms are also provided for principal stress orientation and maximum shear stress. Instead of operating a traditional large-sided photoelasticscope, a compact optic system using a He-Ne laser as a light source is installed on an optic bench to obtain the experimental results for the testing of the disk in diametral distributed compression. Full-field comparisons of isochromatic/isoclinic fringes between testing and theory are presented. The validity of using isochromatic fringes to interpret the maximum shear stress for disks subjected to partially distributed compression is discussed in detail.

Full Field Analytical Solutions for Disks in Partially Distributed Compressions

Consider a circular disk loaded by two diametrically opposing distributed compressive forces located on the top and bottom of the disk. The geometric configuration of this problem is shown in Fig. 1. Hondros used a polar coordinate system to present the full-field stresses in a series solution and the results are expressed as follows:

$$\sigma_r = -\frac{2p}{\pi}\left\{\alpha + \sum_{n=1}^{n=\infty}\left[1-\left(1-\frac{1}{n}\right)\rho^2\right]\rho^{2n-2}\sin 2n\alpha\cos 2n\theta\right\} \quad (1)$$

$$\sigma_\theta = -\frac{2p}{\pi}\left\{\alpha - \sum_{n=1}^{n=\infty}\left[1-\left(1+\frac{1}{n}\right)\rho^2\right]\rho^{2n-2}\sin 2n\alpha\cos 2n\theta\right\} \quad (2)$$

K.-M. Hung was a Graduate Student and C.-C. Ma (ccma@ntu.edu.tw) is a Professor, Department of Mechanical Engineering, National Taiwan University, Taipei, Taiwan 10617, Republic of China. K.-M. Hung now is an Associate Professor, Hwa-Hsia College of Technology and Commerce, Tripei, Taiwan, 23554, Republic of China.

Original manuscript submitted: December 7, 2001.
Final manuscript received: January 9, 2003.

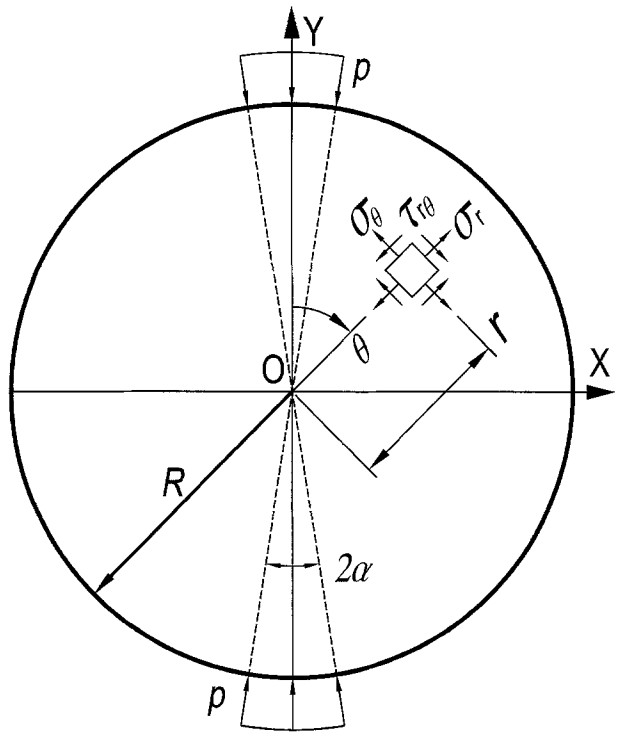

Fig. 1—A circular disk subjected to diametral distributed compression

$$\tau_{r\theta} = \frac{2p}{\pi}\left\{\sum_{n=1}^{n=\infty}\left[1-\rho^2\right]\rho^{2n-2}\sin 2n\alpha \sin 2n\theta\right\}. \quad (3)$$

Here, p is the applied load to be expressed as pressure, 2α is the angle at the origin subtended by the loaded section of the rim, R is the radius of disk, and ρ is equal to r/R.

We illustrate in detail how to derive σ_r in a compact analytical form as follows. First, all the trigonometric functions are decomposed into a unique sine function which is equal to the image part of Euler's formulae,

$$\begin{aligned}\sigma_r &= -\frac{2p}{\pi}\left\{\alpha + \sum_{n=1}^{n=\infty}\left[\rho^{-2}-1+\frac{1}{n}\right]\rho^{2n}\right.\\ &\qquad \left.\frac{\sin 2n(\alpha+\theta)+\sin 2n(\alpha-\theta)}{2}\right\}\\ &= -\frac{p}{\pi}\left\{2\alpha + (\rho^{-2}-1)\sum_{n=1}^{n=\infty}\rho^{2n}\right.\\ &\qquad \mathrm{Im}\left[e^{i2n(\alpha+\theta)}+e^{i2n(\alpha-\theta)}\right]\\ &\qquad \left.+\sum_{n=1}^{n=\infty}\frac{1}{n}\rho^{2n}\,\mathrm{Im}\left[e^{i2n(\alpha+\theta)}+e^{i2n(\alpha-\theta)}\right]\right\}. \end{aligned} \quad (4)$$

Because $\sum_{n=1}^{n=\infty}\rho^{2n}e^{i2n(\alpha\pm\theta)}$ is a geometric series and is convergent since $|\rho^2 e^{i2(\alpha\pm\theta)}| < 1$, the second term of eq (4) is written as

$$\begin{aligned}&(\rho^{-2}-1)\sum_{n=1}^{n=\infty}\rho^{2n}\mathrm{Im}\left[e^{i2n(\alpha+\theta)}+e^{i2n(\alpha-\theta)}\right]\\ &= (1-\rho^2)\left[\frac{\sin 2(\alpha+\theta)}{\rho^4+1-2\rho^2\cos 2(\alpha+\theta)}\right.\\ &\qquad \left.+\frac{\sin 2(\alpha-\theta)}{\rho^4+1-2\rho^2\cos 2(\alpha-\theta)}\right]. \end{aligned} \quad (5)$$

According to $\frac{1}{n}\rho^{2n}e^{i2n(\alpha\pm\theta)} = i\int\rho^{2n}e^{i2n(\alpha\pm\theta)}d(2\alpha)$, the third term of eq (4) is written as

$$\begin{aligned}&\mathrm{Im}\sum_{n=1}^{n=\infty}\frac{1}{n}\rho^{2n}\left[e^{i2n(\alpha+\theta)}+e^{i2n(\alpha-\theta)}\right]\\ &= \mathrm{Im}\left[i\int\sum_{n=1}^{n=\infty}\rho^{2n}e^{i2n(\alpha+\theta)}d(2\alpha)\right.\\ &\qquad \left.+i\int\sum_{n=1}^{n=\infty}\rho^{2n}e^{i2n(\alpha-\theta)}d(2\alpha)\right]\\ &= \int\frac{-\rho^4+\rho^2\cos 2(\alpha+\theta)}{\rho^4+1-2\rho^2\cos 2(\alpha+\theta)}d(2\alpha)\\ &\qquad +\int\frac{-\rho^4+\rho^2\cos 2(\alpha-\theta)}{\rho^4+1-2\rho^2\cos 2(\alpha-\theta)}d(2\alpha). \end{aligned} \quad (6)$$

The integration of eq (6) can be worked out as follows:

(i) For $0 \le \theta \le \pi/2-\alpha$.

Recalling the formula[9]

$$\begin{aligned}\int\frac{A+B\cos X}{a+b\cos X}dX &= \frac{B}{b}X\\ &+\frac{Ab-aB}{b}\frac{2}{\sqrt{a^2-b^2}}\tan^{-1}\left[\frac{\sqrt{a^2-b^2}}{a+b}\tan\frac{X}{2}\right], \end{aligned} \quad (7)$$

where $a^2 > b^2$. Setting $A = -\rho^4$, $B = \rho^2$, $a = (\rho^4+1)$, $b = -2\rho^2$, and $X = 2(\alpha\pm\theta)$, the integration of eq (6) is calculated to be

$$\begin{aligned}&-2\alpha+\tan^{-1}\left[\frac{1+\rho^2}{1-\rho^2}\tan(\alpha+\theta)\right]\\ &+\tan^{-1}\left[\frac{1+\rho^2}{1-\rho^2}\tan(\alpha-\theta)\right]. \end{aligned} \quad (8)$$

(ii) For $\pi/2-\alpha \le \theta \le \pi/2$.

As $\theta = \pi/2-\beta$ and $0 \le \beta \le \alpha$, the integration of eq (6) is written as

$$\begin{aligned}&\int\frac{-\rho^4-\rho^2\cos 2(\alpha-\beta)}{\rho^4+1+2\rho^2\cos 2(\alpha-\beta)}d(2\alpha)\\ &+\int\frac{-\rho^4-\rho^2\cos 2(\alpha+\beta)}{\rho^4+1+2\rho^2\cos 2(\alpha+\beta)}d(2\alpha). \end{aligned} \quad (9)$$

Recalling eq (7) and letting $A = -\rho^4$, $B = -\rho^2$, $a = (\rho^4 + 1)$, $b = 2\rho^2$, $X = 2(\alpha \pm \beta)$, the integration of eq (9) is expressed as

$$-2\alpha + \pi + \tan^{-1}\left[\frac{1+\rho^2}{1-\rho^2}\tan(\alpha+\theta)\right] + \tan^{-1}\left[\frac{1+\rho^2}{1-\rho^2}\tan(\alpha-\theta)\right]. \tag{10}$$

Introducing eqs (5), (8) and (10) to eq (4), the analytical solution of σ_r is derived as a simple closed form without summation

$$\sigma_r(r,\theta) = -\frac{p}{\pi}\left\{\begin{array}{l}(1-\rho^2)\left[\dfrac{\sin 2(\alpha+\theta)}{\rho^4+1-2\rho^2\cos 2(\alpha+\theta)} + \dfrac{\sin 2(\alpha-\theta)}{\rho^4+1-2\rho^2\cos 2(\alpha-\theta)}\right] \\ +\tan^{-1}\left[\dfrac{1+\rho^2}{1-\rho^2}\tan(\alpha+\theta)\right] \\ +\tan^{-1}\left[\dfrac{1+\rho^2}{1-\rho^2}\tan(\alpha-\theta)\right] + \Phi\end{array}\right\} \tag{11}$$

$$0 \le \theta \le \frac{\pi}{2},$$

where

$$\Phi = \begin{cases} 0 & \text{for } 0 \le \theta \le \frac{\pi}{2} - \alpha \\ \pi & \text{for } \frac{\pi}{2} - \alpha \le \theta \le \frac{\pi}{2} \end{cases}.$$

The procedures to derive σ_θ are similar to those for σ_r and the analytical solution for σ_θ is obtained as

$$\sigma_\theta(r,\theta) = -\frac{p}{\pi}\left\{\begin{array}{l}-(1-\rho^2)\left[\dfrac{\sin 2(\alpha+\theta)}{\rho^4+1-2\rho^2\cos 2(\alpha+\theta)} + \dfrac{\sin 2(\alpha-\theta)}{\rho^4+1-2\rho^2\cos 2(\alpha-\theta)}\right] \\ +\tan^{-1}\left[\dfrac{1+\rho^2}{1-\rho^2}\tan(\alpha+\theta)\right] \\ +\tan^{-1}\left[\dfrac{1+\rho^2}{1-\rho^2}\tan(\alpha-\theta)\right] + \Phi\end{array}\right\} \tag{12}$$

$$0 \le \theta \le \frac{\pi}{2}.$$

Similar to deriving the second term of eq (4), the full-field analytical solution of $\tau_{r\theta}$ is represented as

$$\tau_{r\theta}(r,\theta) = \frac{2p}{\pi}\left\{\sum_{n=1}^{n=\infty}\left[\rho^{-2}-1\right]\rho^{2n} \frac{\cos 2n(\alpha-\theta) - \cos 2n(\alpha+\theta)}{2}\right\} \tag{13}$$

$$= \frac{p}{\pi}\left\{(1-\rho^2)\left[\frac{-\rho^2+\cos 2(\alpha-\theta)}{\rho^4+1-2\rho^2\cos 2(\alpha-\theta)} - \frac{-\rho^2+\cos 2(\alpha+\theta)}{\rho^4+1-2\rho^2\cos 2(\alpha+\theta)}\right]\right\}.$$

Figures 2(a), (b) and (c) are contour plots based on three dimensionless solutions σ_r/p, σ_θ/p, $\tau_{r\theta}/p$ for a small angle $\alpha = 4.5°$. Figures 3(a)–(c) are contour plots for a large angle $\alpha = 60°$. Obviously, the contour plots between small and large angles are quite different.

For $\alpha = 90°$, the solutions will reduce to the problem of a uniform radial traction with intensity p and the results are $\sigma_r = -p$, $\sigma_\theta = -p$, and $\tau_{r\theta} = 0$ for the whole field. When $\alpha = 0°$, it is the ideal case of a disk subjected to a concentrated force acting along the diameter. Letting $p = \frac{P}{2\alpha Rt}$, and taking the limit as $\alpha \to 0$, then the analytical solutions of the concentrated force problem are derived as follows:

$$\sigma_r|_{\alpha\to 0} = \lim_{\alpha\to 0} -\frac{P}{2\pi Rt}\frac{1}{\alpha} \tag{14}$$

$$\left\{\begin{array}{l}(1-\rho^2)\left[\dfrac{\sin 2(\alpha+\theta)}{\rho^4+1-2\rho^2\cos 2(\alpha+\theta)} + \dfrac{\sin 2(\alpha-\theta)}{\rho^4+1-2\rho^2\cos 2(\alpha-\theta)}\right] \\ +\tan^{-1}\left[\dfrac{1+\rho^2}{1-\rho^2}\tan(\alpha+\theta)\right] \\ +\tan^{-1}\left[\dfrac{1+\rho^2}{1-\rho^2}\tan(\alpha-\theta)\right] + \Phi\end{array}\right\} = \frac{P}{\pi Rt}\left\{\frac{(1-\rho^2)^2(\rho^4+2\rho^2-1-2\cos 2\theta)}{(\rho^4+1-2\rho^2\cos 2\theta)^2}\right\}$$

$$\sigma_\theta|_{\alpha\to 0} = \frac{P}{\pi Rt}\left\{\frac{\rho^8+4\rho^4-4\rho^2-1+2(-2\rho^6+\rho^4+1)\cos 2\theta)}{(\rho^4+1-2\rho^2\cos 2\theta}\right\} \tag{15}$$

$$\tau_{r\theta}|_{\alpha\to 0} = \frac{P}{\pi Rt}\left\{\frac{2(1-\rho^4)(1-\rho^2)\sin 2\theta)}{(\rho^4+1-2\rho^2\cos 2\theta}\right\} \tag{16}$$

where t is the thickness of the disk and P is the applied concentrated force. All solutions expressed in eqs (14)–(16) are the same as those presented by Sokolnikoff[4] with only a negative sign appearing at $\tau_{r\theta}$ to represent a different definition of the orientation of θ.

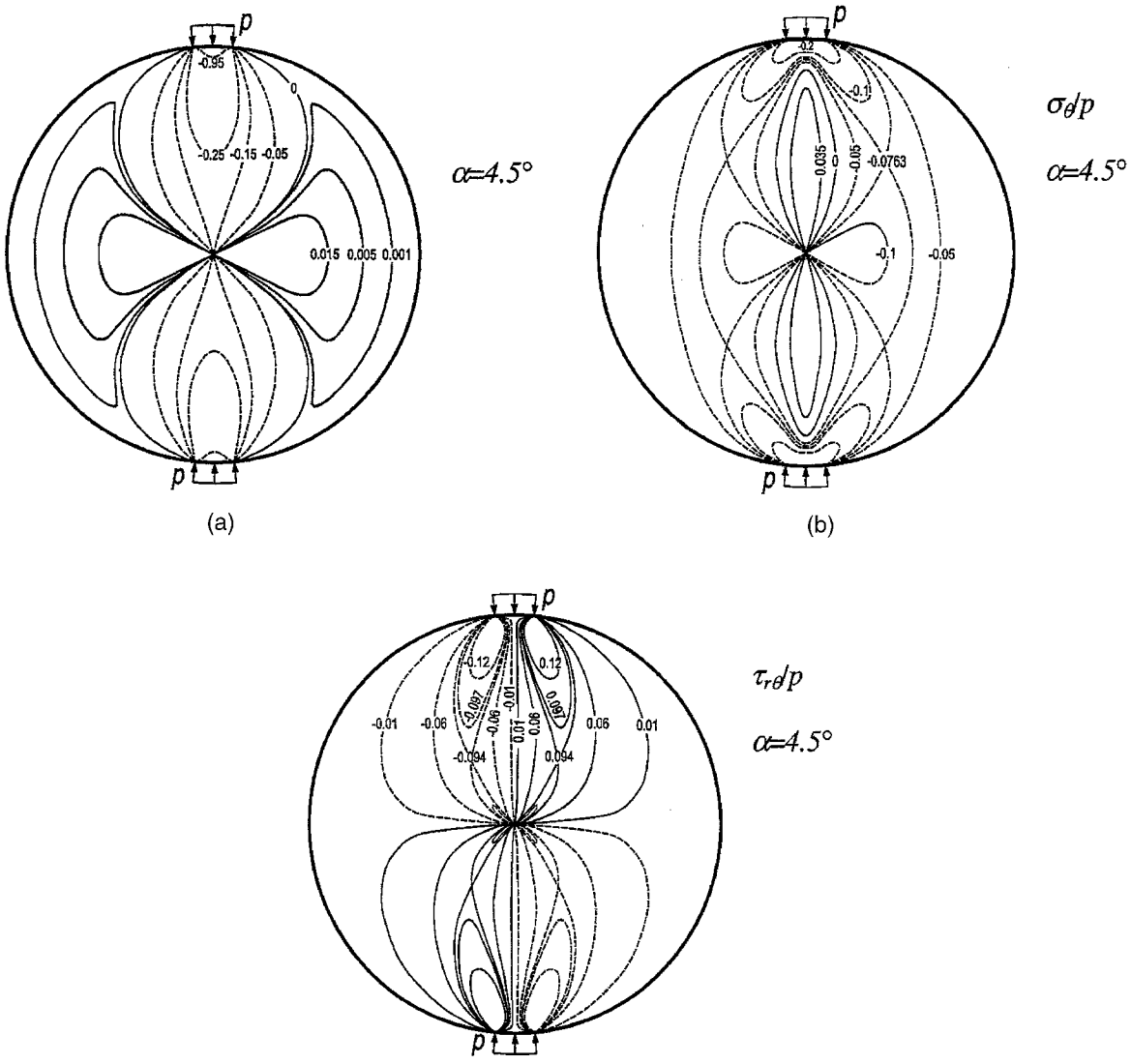

Fig. 2—(a) $\alpha = 4.5°$, σ_r/p contours; (b) $\alpha = 4.5°$, σ_θ/p contours; (c) $\alpha = 4.5°$, $\tau_{r\theta}/p$ contours

Experimental Results

A compact, collimated-light, digital photoelastic system consisting of two subsystems is shown schematically in Fig. 4. The collimated light subsystem for projecting the specimen image on a ground glass includes a He-Ne laser, a spatial filter, and a parabolic mirror. The CCD camera acquires an isochromatic fringe image through a frame grabber and displays it on the monitor of a personal computer in real time.

A disk subjected to diametral distributed forces is stress frozen using conventional procedures and is examined by using the compact digital photoelastic system mentioned above. The disk diameter is 76 mm, the thickness is 8 mm and the loading range α is about 4.5°.

Isoclinics

The isoclinic fringes are the loci of points where the principal stress directions coincide with the axis of the polarizer. Letting θ_P be the angle between the x-axis and the principal stress orientation, we have

$$\theta_P = \frac{1}{2}\tan^{-1}\left[\frac{\frac{\sigma_r - \sigma_\theta}{2}\sin 2\theta + \tau_{r\theta}\cos 2\theta}{-\frac{\sigma_r - \sigma_\theta}{2}\cos 2\theta + \tau_{r\theta}\sin 2\theta}\right] = \frac{1}{2}\tan^{-1}\left[\frac{2\rho^2\cos 2\alpha\sin 2\theta - \rho^4\sin 4\theta}{1 - 2\rho^2\cos 2\alpha\cos 2\theta + \rho^4\cos 4\theta}\right]. \quad (17)$$

Although the analytical solutions for stresses σ_r, σ_θ, $\tau_{r\theta}$ are functions possessing very complicated forms as shown in eqs (11), (12) and (13), respectively, the principal stress orientation θ_P can be concisely represented by eq (17) which is regarded as the isoclinic equation for the disk subjected to distributed compression. As $\alpha = 0°$, eq (17) reduces to

$$\theta_P = \frac{1}{2}\tan^{-1}\left[\frac{2\rho^2\sin 2\theta - \rho^4\sin 4\theta}{1 - 2\rho^2\cos 2\theta + \rho^4\cos 4\theta}\right]. \quad (18)$$

Equation (18) is the principal stress orientation equation for the problem of a disk subjected to concentrated forces acting

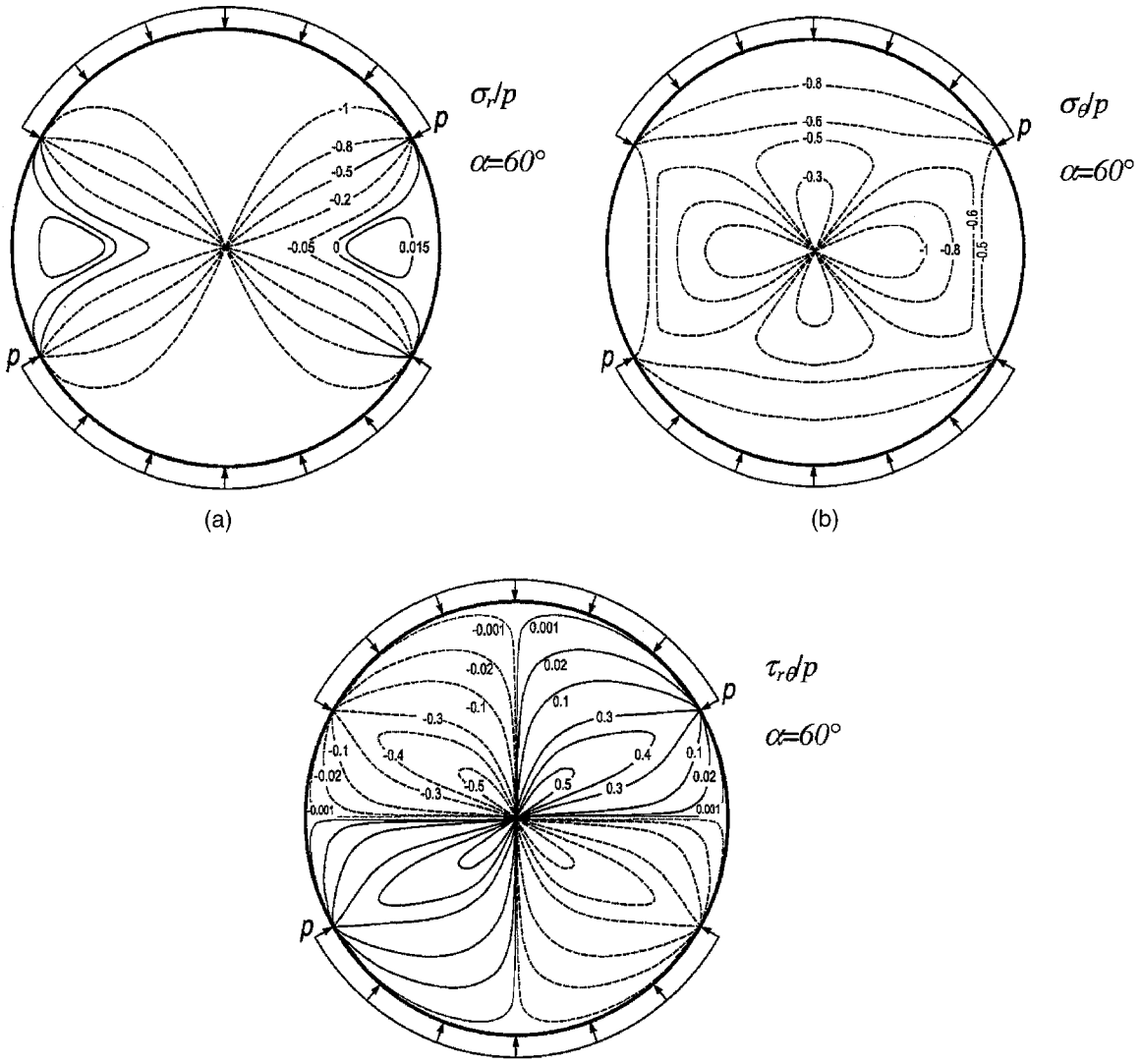

Fig. 3—(a) $\alpha = 60°$, σ_r/p contours; (b) $\alpha = 60°$, σ_θ/p contours; (c) $\alpha = 60°$, $\tau_{r\theta}/p$ contours

along the diameter. Figure 5 shows the theoretical isoclinic contour plot. The comparisons of isoclinic fringes between theoretical and experimental images are shown in Fig. 6 for the orientation angle $\theta_P = 45°$.

Isochromatics and the Maximum Shear Stress

For the two-dimensional problem considered in this paper, we have the condition $\sigma_z = \tau_{zr} = \tau_{z\theta} = 0$ and a state of plane stress exists. The three principal stresses are

$$\sigma_1, \sigma_2 = \frac{\sigma_r + \sigma_\theta}{2} \pm \sqrt{\left(\frac{\sigma_r - \sigma_\theta}{2}\right)^2 + \tau_{r\theta}^2}, \qquad (19)$$

$$\sigma_3 = 0,$$

where σ_1 and σ_2 are the principal stresses in the plane of the specimen. The maximum shear stress is given by

$$\tau_{\max} = \frac{1}{2}(\sigma_1 - \sigma_2) \qquad (20)$$

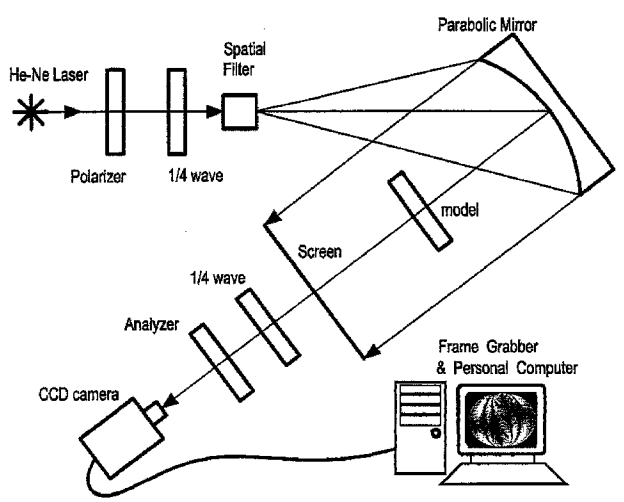

Fig. 4—A compact collimated-light digital photoelastic system

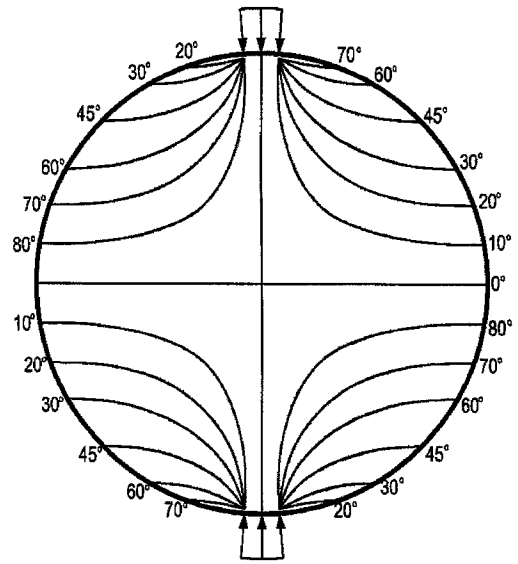

Fig. 5—Theoretical isoclinic contours for distributed compression

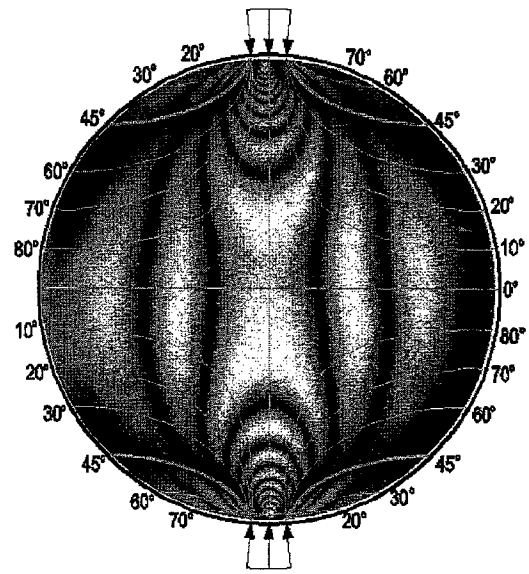

Fig. 6—45° isoclinic fringes for $\alpha = 4.5°$

provided σ_1 and σ_2 are of opposite sign and $\sigma_3 = 0$; otherwise

$$\tau_{max} = \begin{cases} \sigma_1/2 & \text{if } \sigma_1 > 0 \text{ and } \sigma_2 > 0 \\ |\sigma_2|/2 & \text{if } \sigma_1 < 0 \text{ and } \sigma_2 < 0 \end{cases}. \quad (21)$$

The maximum shear stress theory of failure is often used in the design of structures and a detailed investigation of the maximum shear stress is needed. The full-field solutions of stresses σ_r, σ_θ, and $\tau_{r\theta}$ are already expressed in eqs (11), (12) and (13), respectively. The principal stresses can be worked out as a simple form

$$\sigma_1, \sigma_2 = -\frac{p}{\pi}\left\{\tan^{-1}\left[\frac{1+\rho^2}{1-\rho^2}\tan(\alpha+\theta)\right] + \tan^{-1}\left[\frac{1+\rho^2}{1-\rho^2}\tan(\alpha-\theta)\right] + \Phi\right\} \pm \frac{2p}{\pi}(1-\rho^2)\sin 2\alpha \frac{1}{\sqrt{\rho^4 - 2\rho^2\cos 2(\alpha+\theta)+1}\sqrt{\rho^4 - 2\rho^2\cos 2(\alpha-\theta)+1}}. \quad (22)$$

It is noted that the first term in eq (22) is negative, hence the principal stress σ_2 is always negative, while σ_1 may be positive or negative depending on ρ, θ and α. When $\sigma_1 > 0$ and $\sigma_2 < \sigma_3 = 0$, the maximum shear stress is one-half the value of $\sigma_1 - \sigma_2$ and can be determined directly from the isochromatic fringe pattern. However, when $\sigma_2 < \sigma_1 < \sigma_3 = 0$, the maximum shear stress is $|\sigma_2|/2$.

The maximum shear stress contour plots for $\alpha = 4.5°$, 30° and 60° are shown in Figs 7(a), (b) and (c), respectively. In these figures, dashed lines indicate the principal stress $\sigma_1 = 0$ which separates the regions that $\sigma_1 > 0$ and $\sigma_1 < 0$ (shaded region). In the unshaded region, the principal stresses $\sigma_1 > 0$ and $\sigma_2 < 0$ are of opposite sign, and the maximum shear stress is determined by $\tau_{max} = |\sigma_1 - \sigma_2|/2$. However, the maximum shear stress is evaluated by $\tau_{max} = |\sigma_2|/2$ in the shaded region since $\sigma_2 < \sigma_1 < 0$. It is also indicated in these figures that the maximum shear stress in the full field for any α never exceeds the value of $0.5p$. The regions (with "+" symbol) where the maximum shear stress equals $0.5p$ are confined in small areas near the applied loadings for small α (see Fig. 7(a) for $\alpha = 4.5°$) and are connected to form a continuous region along the vertical direction for medium values of α (see Fig. 7(b) for $\alpha = 30°$). Finally, this region spreads out near the whole disk as α is large (see Fig. 7(c) for $\alpha = 60°$). When $\alpha = 90°$, the solution will reduce to the case of uniform radial tractions applied in the whole boundary, and we have $\sigma_1 = \sigma_2 = -p$ in the full field so that $\tau_{max} = p/2$ in the entire disk.

The isochromatic fringe pattern gives lines for which the principal stress difference is equal to a constant. The solution of the principal stress difference for the problem of a disk subjected to distributed compression is easily obtained from eq (22) as follows:

$$\frac{\sigma_1 - \sigma_2}{2} = \frac{2p}{\pi}(1-\rho^2)\sin 2\alpha \frac{1}{\sqrt{\rho^4 - 2\rho^2\cos 2(\alpha+\theta)+1}\sqrt{\rho^4 - 2\rho^2\cos 2(\alpha-\theta)+1}}. \quad (23)$$

For the concentrated force problem (i.e., $\alpha = 0$), the analytical full-field solutions for stresses are presented in eqs (14)–(16), and the in-plane principal stresses σ_1 and σ_2 are derived to be

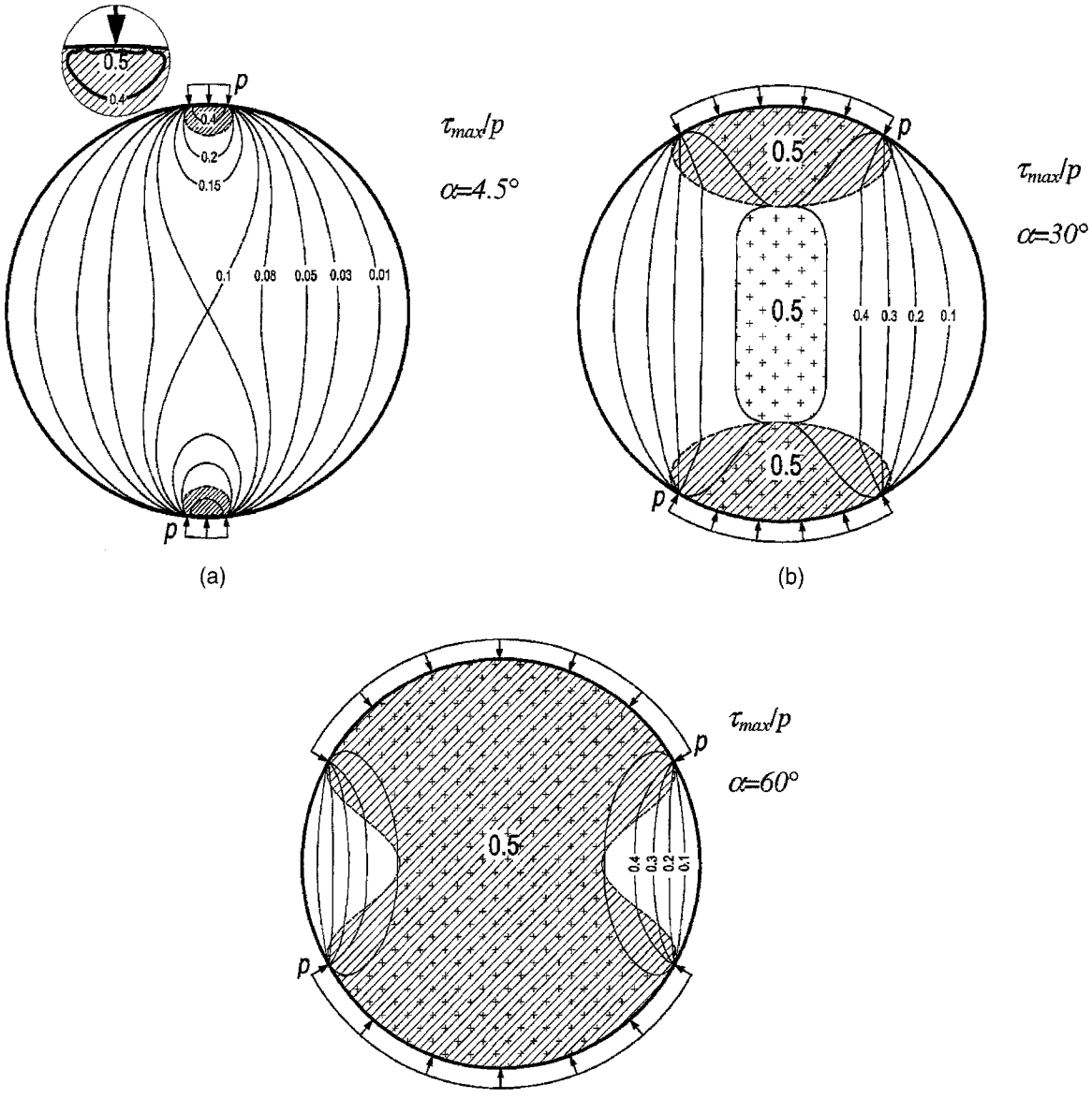

Fig. 7—Contours of dimensionless maximum shear stress τ_{max}/p for (a) $\alpha = 4.5°$, (b) $\alpha = 30°$, (c) $\alpha = 60°$

$$\sigma_1 = \frac{P}{\pi R t}\frac{(\rho^2-1)^2}{\rho^4+1-2\rho^2\cos 2\theta},$$
$$\sigma_2 = \frac{P}{\pi R t}\frac{\rho^4+2\rho^2-3}{\rho^4+1-2\rho^2\cos 2\theta}. \quad (24)$$

It is easy to see from eq (24) that $\sigma_1 \geq 0$ and $\sigma_2 \leq 0$ in the entire disk and the maximum shear stress is determined by the difference of principal stresses as follows

$$\tau_{max} = \frac{\sigma_1-\sigma_2}{2} = \frac{2P}{\pi R t}\frac{1-\rho^2}{\rho^4+1-2\rho^2\cos 2\theta}. \quad (25)$$

Figure 8 shows a contour plot of dimensionless principal stress difference $(\sigma_1 - \sigma_2)/2P$ for $\alpha = 4.5°$. It is clearly shown in Fig. 8 that the maximum principal stress difference is moved from the boundary and produces a local fringe near the boundary. For truly concentrated loads, the fringes originate at the points of application of the loads. Figure 9(a) shows the image pattern after taking the absolute value from the difference between the dark field image and the light field image with the number of fringe increased. Each dark isochromatic has a fringe order of $N = 0.25, 0.75, 1.25\ldots$. Figure 9(b) shows a comparison between the simulation image by using eq (23) and Fig. 9(a) in the same figure. Obviously, the analytical solution and experimental results match very well.

Conclusions

In the development of photoelasticity, the disk in diametral compression is an important model to be utilized to illustrate new theories and experimental techniques. The compression is usually idealized to be concentrated forces of reverse direction mainly because it can be compared with the theoretical

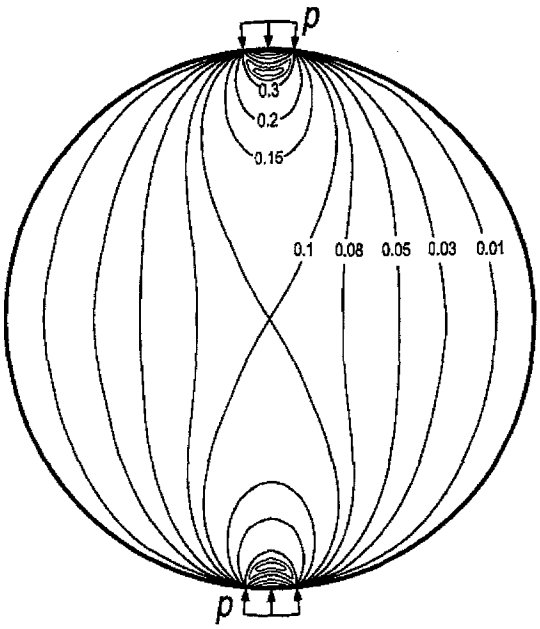

Fig. 8—Contours of dimensionless principal stress difference $(\sigma_1 - \sigma_2)/2p$ for $\alpha = 4.5°$

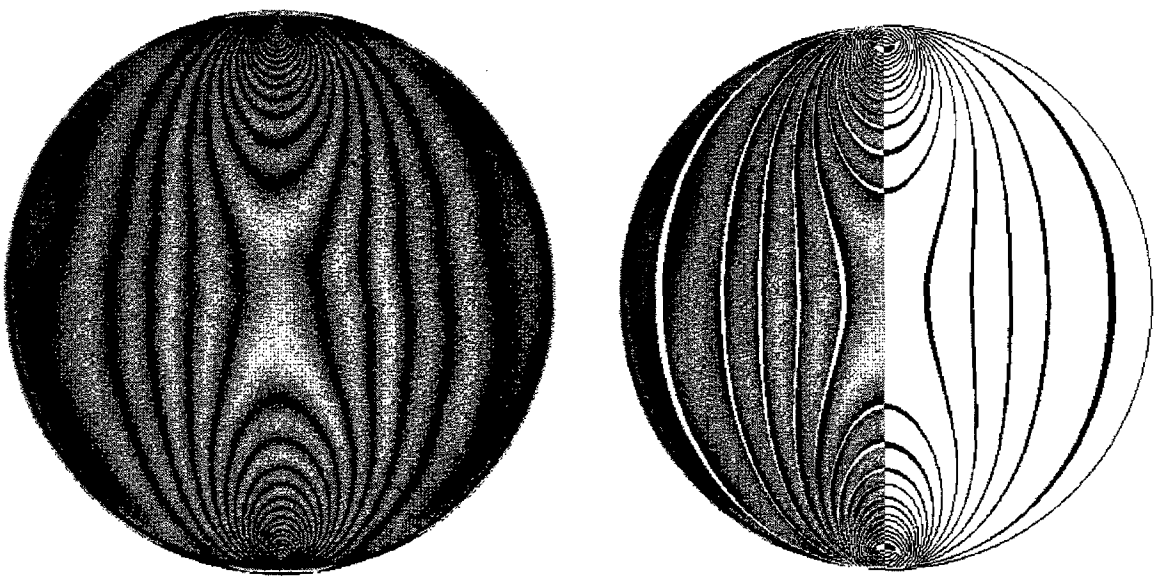

(a) (b)

Fig. 9—(a) Fringe multiplication for isochromatic image and (b) comparison image between theoretical predication and experimental result

solution. However, a disk in diametral compression on a small area is an experimental condition very close to reality and there is a lack of a theoretical solution expressed in a concise form. In this paper we extend the contribution of Hondros[8] by deriving an analytical solution for the full-field stress for the problem of a disk in diametral compression on a finite area at the rim. This provides a theoretical model for comparing the full-field data sampling of a disk in distributed compression in future work. The pithy forms of principal stresses and principal stress orientation are also derived to offer engineering application. The maximum shear stress for the whole disk is derived and is also discussed in detail. Furthermore, a compact optical system for digital photoelasticity is operated to acquire the digital image of isochromatics and isoclinics for a disk in diametral distributed compression. The isochromatic fringes are in good agreement with the theoretical ones in terms of the full field. It is also indicated in this study that the isochromatic fringes cannot be used to interpret the maximum shear stress if the angle of the distributed compression is large. The isochromatic fringes in the whole field are identical to the maximum shear stress only for the disk subjected to diametral concentrated forces.

Acknowledgments

We gratefully acknowledge the financial support of the National Science Council, Republic of China, under Grant NSC 89-2218-E002-034 at National Taiwan University. We appreciate helpful discussions with Professor Chwei-Goong Tseng at National Taiwan University of Science and Technology.

References

1. Frocht, M.M., Photoelasticity, Vol. II, Wiley, New York, 131–155 (1948).

2. Timoshenko, S. and Goodier, J.N., Theory of Elasticity, 2nd edition McGraw-Hill, New York, Sec. 41 (1951).

3. Muskhelishvili, N.I., Some Basic Problems of the Mathematical Theory of Elasticity, Noordhoff International Publishing, The Netherlands (1975).

4. Sokolnikoff, I.S., Mathematical Theory of Elasticity, McGraw-Hill, New York, 283–284 (1956).

5. Sanford, R.J., "Application of the Least-squares Method to Photoelastic Analysis," EXPERIMENTAL MECHANICS, **20** *(6), 192–197 (1980).*

6. Berghaus, D.G., "Combining Photoelasticity and Finite-element Methods for Stress Analysis Using Least Squares," EXPERIMENTAL MECHANICS, **31** *(1), 36–41 (1991).*

7. Haake, S.J., Patterson, E.A., and Wang, Z.F., "2D and 3D Separation of Stresses Using Automated Photoelasticity," EXPERIMENTAL MECHANICS, **36** *(3), 269–276 (1996).*

8. Hondros, G., "The Evaluation of Poisson's Ratio and the Young's Modulus of Materials of a Low Tensile Resistance by the Brazilian Test," Austral. J. Appl. Sci., **10** *(3), 243–268 (1959).*

9. Gradshteyn, I.S. and Ryzhik, I.M., Table of Integrals, Series, and Products, Academic, New York, 148 (1980).